2011 International Symposium on Nonlinear Theory and its Applications
NOLTA2011, Kobe, Japan, September 4-7, 2011

Optimal entrainment of limit-cycle oscillators and its applications to communication devices

Hisa-Aki Tanaka, Naotaka Sagayama, Takahiro Harada†, and István Z. Kiss‡

Graduate School of Information Systems, UEC, Tokyo, 182-8585 Japan
†Department of Physics, The University of Tokyo, Tokyo 113-0033 Japan
‡Department of Chemistry, Saint Louis University, St. Louis, MO 63103 USA

Abstract—A general theory for designing optimal, energy-efficient injection-locking oscillators is presented. Phase model analysis is combined with variational analysis to derive an injection signal with which frequency-locking of an oscillator is achieved with minimum power injection signal. Optimal signal waveforms are calculated from the phase response curve (the impulse sensitivity function) and a solution to a balancing condition. The theory is tested in various numerical experiments in which oscillations close to and further away from a Hopf bifurcation exhibited nearly sinusoidal and non-sinusoidal optimal waveforms, respectively. Applications of the theory are developed for practical high frequency oscillators, which are quite useful for designing new energy-efficient hardwares in communication devices.

1. Introduction

Entrainment of oscillators to an external signal in nonlinear dissipative systems is a fundamental concept of importance in a large variety of applications [1]; two prominent examples in nonlinear sciences include the time-scale adjustment of circadian system to light [2] and the cardiac system to a pacemaker [3]. In electrical engineering, this concept of entrainment of oscillators has been known as injection-locking. Interestingly, this classical concept of injection-locking has gained more and more attention these several years, since this technique requires less power, compared with the conventional power-consuming PLL technique. For instance, in 2006 [4] presented 70GHz CMOS injection-locked divider at 2006 IEEE ISSCC. Also, in 2008, 4.8GHz CMOS pulse-injection locking frequency multiplier is reported in [5]. Finally in 2010 researchers in Sony presented their base-band communication device using injection-locking oscillators at 2010 ISSCC. Namely, these techniques have their common advantages in their circuit simplicity and power-efficiency, which is essential in high frequency operation for ICT. However, theoretical insight of these techniques, and also their optimization, has never been obtained so far.

The injection-locking (entrainment) process has been described theoretically by phase/amplitude equations and circle maps for weakly and strongly perturbed nonlinear systems, respectively [1]. The general result of the theoretical analysis is that nonlinear oscillators can adjust their frequencies to that of the external source (injection signal) above a critical forcing amplitude. In the forcing amplitude vs. forcing frequency diagram there are long vertical entrainment regions called Arnold tongues. A widely accepted tool for studying entrainment is the phase response curve [2]. Specifically, the phase response function (infinitesimal phase response curve) indicates the phase shift of an oscillator due to an infinitesimal perturbation of a system variable [8]. A classical problem in nonlinear dynamics uses phase response function and forcing waveform with which all important features of the entrainment process (e.g., locking range, defined as the width of the Arnold tongue at a given forcing amplitude) can be obtained for weakly perturbed systems [1]. It should be noted that the above concepts of 'phase equation' and 'phase response function' have been known as 'the Adler's equation [6]' and 'impulse sensitivity function [7]' respectively, and these are important foundations of injection-locking.

Many applications require optimization of the entrainment process. This is often achieved by adjusting the forcing waveform to achieve a target entrainment feature. A variety of control targets were explored: optimal input was determined for establishing fast entrainments [9], circadian phase resetting [10, 11], starting/stopping of the oscillations [11, 12], and maximal resonance (energy transfer) between the system and forcing signal [13]. Control of deterministic [14] and stochastic [16, 15] neuronal spiking activity was achieved with phase modeling approach combined with variational methods to optimize spiking time [14] and variance of firing rates [16].

In this study, we give a theoretical foundation for the inverse of the classical entrainment problem: what is the minimal power injection waveform that produces power-efficient entrainment of a limit-cycle oscillator in weak injection conditions? Although the quality of entrainment could involve features such as stability and basin of attraction, here we consider efficient entrainment as the occurrence of maximum width (or minimum slopes) of the Arnold tongue. This 'locking range' quality marker has been commonly used for injection-locking oscillators as well as phase-locked loop circuits [17]. We propose a versatile, efficient approach to obtain exact functional form of the optimal waveform provided that the response func-

tion related to the forcing action had been established. The theoretically obtained optimal injection waveforms, which exhibit some unexpected symmetry relationships with the phase response function, are tested in a simple numerical model that include higher harmonics in the response function typically seen in strongly nonlinear oscillators.

2. Mathematical modeling of entrainment

The entrainment process of a limit-cycle oscillator in weak forcing limit can be modeled by [18]

$$\frac{d\psi}{dt} = \omega + Z(\psi) f(\Omega t), \tag{1}$$

where ψ is the phase of the oscillator, Z is the phase response function, and ω and Ω are the natural frequency of the oscillator and the forcing frequency, respectively. In weak forcing limit, Eq. (1) is further simplified by averaging [19], as

$$\frac{d\phi}{dt} = \Delta\omega + \Gamma(\phi), \tag{2}$$

where ϕ and $\Delta\omega$ are given by $\phi = \psi - \Omega t$, and $\Delta\omega = \Omega - \omega$, respectively [20]. The interaction function, $\Gamma(\phi)$, is obtained from the forcing waveform f and the phase response function, Z, as $\Gamma(\phi) = \langle Z(\theta+\phi) f(\theta)\rangle$, where θ represents Ωt and $\langle\cdot\rangle$ denotes the average by θ over its period 2π: $\langle\cdot\rangle \equiv (2\pi)^{-1}\oint\cdot\, d\theta$. It is noted that Eq. (2) has been known as the Adler's equation [6]. Entrainment occurs when the phase difference is locked, i.e., $d\phi/dt = \Delta\omega + \Gamma(\phi) = 0$ [11]. The range of frequency difference, $\Delta\omega$, where solution for stable steady state exists for ϕ defines the locking range $R[f]$ for a certain forcing waveform [21]. Therefore, the locking range is the difference between the maximum (at $\phi = \phi_+$) and minimum (at $\phi = \phi_-$) values of $\Gamma(\phi)$ where phase locked solution exists [22]. $R[f]$ is thus given by $\Gamma(\phi_+) - \Gamma(\phi_-)$ as shown in Fig. 2.

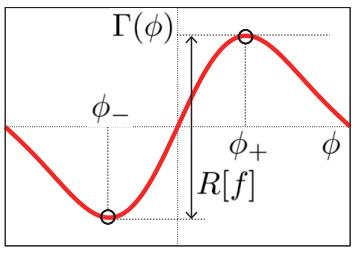

Figure 1: The locking range $R[f]$ defined by the difference between the maximum ($\Gamma(\phi_+)$) and minimum ($\Gamma(\phi_-)$).

3. Variational calculation for optimal forcing waveforms

Now we are in position to formulate the optimal entrainment problem mathematically: the optimal forcing waveform ($f_{\rm opt}$) maximizes the locking range R under certain constraints. A convenient practical constraint is the total power of the waveform over its period: $\langle f(\theta)^2\rangle$. Therefore, the optimal forcing waveform, $f_{\rm opt}$ gives maximal locking range for a given (constant) forcing power P. We consider this as a variational problem maximizing the functional form

$$\mathcal{S}[f] \equiv R[f] - \lambda(\langle f^2\rangle - P), \tag{3}$$

where λ is the Lagrange multiplier. Solution to the variational problem, f_*, a suitable candidate for the optimal waveform, is obtained by ensuring that the first variation $\delta\mathcal{S}$ vanishes and the second variation $\delta^2\mathcal{S}$ is negative [23]:

$$f_*(\theta) = (2\lambda)^{-1}\{Z(\theta+\phi_+) - Z(\theta+\phi_-)\}. \tag{4}$$

The Lagrange multiplier can be obtained by substituting the solution Eq. (4) in the constant power constraint ($\langle f_*^2\rangle - P = 0$): $\lambda = (1/2)\sqrt{Q/P}$ with $Q \equiv \langle\{Z(\theta+\phi_+) - Z(\theta+\phi_-)\}^2\rangle$. Note that f_* in Eq. (4) has zero average: $\langle f_*\rangle = 0$.

To obtain f_* of Eq. (4) the maximum (ϕ_+) and the minimum (ϕ_-) ϕ values of Γ with the forcing waveform

$$\Gamma(\phi) = \sqrt{P/Q}\,\langle Z(\theta+\phi)\{Z(\theta+\phi_+) - Z(\theta+\phi_-)\}\rangle \tag{5}$$

have to be determined. The conditions for the maximum and minimum of Γ are as follows:

$$\Gamma'(\phi_\pm) = 0,\ \Gamma''(\phi_+) < 0,\ \text{and}\ \Gamma''(\phi_-) > 0. \tag{6}$$

The first condition in Eqs. (6), combined with Eq. (5), gives

$$\langle Z'(\theta+\phi_+)Z(\theta+\phi_-)\rangle = \langle Z'(\theta+\Delta\phi)Z(\theta)\rangle = 0 \tag{7}$$

where $\Delta\phi \equiv \phi_+ - \phi_-$. ($\Delta\phi$ is introduced to remove phase ambiguity). We shall refer to Eq. (7) as balancing condition because this equation realizes optimality by balancing both terms in Eq. (4). The trivial $\Delta\phi = 0$ solution to Eq. (7) is discarded because it does not allow entrainment ($\Gamma(\phi) \equiv 0$ in Eq. (5)).

However, other solutions do exist in Eq. (7), because $\partial\langle Z'(\theta+\Delta\phi)Z(\theta)\rangle/\partial\Delta\phi|_{\Delta\phi=0} = -\langle Z'(\theta)^2\rangle < 0$, and $\langle Z'(\theta+\Delta\phi)Z(\theta)\rangle$ is a periodic, bounded function of $\Delta\phi$ in a large class of systems [1]. In particular, we have found that in models with twice differentiable, continuous Z a solution with $\Delta\phi = \pi$ exists; we call this solution and the corresponding optimal waveform 'generic' [25].

4. Numerical verification of theoretical predictions

Here we test the above theoretical predictions by a simple model with the following response function,

$$Z(\theta) = \sin\theta + a\sin(2\theta). \tag{8}$$

This Z simulates the behavior of Stuart-Landau oscillator [1] with $a = 0$; therefore, we can consider a as a measure of distance from Hopf bifurcation that can introduce

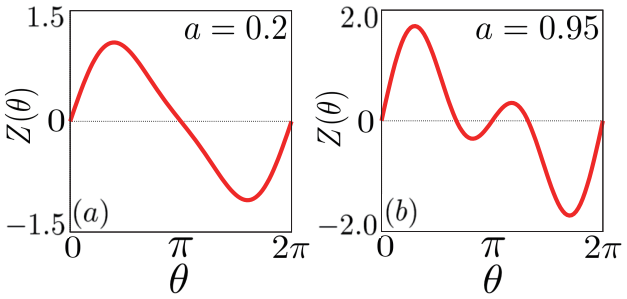

Figure 2: Phase response function $Z(\theta)$ of Eq. (8). Panel (a) represents the case of near Hopf bifurcation point. Panel (b) represents the case being far away from Hopf bifurcation point.

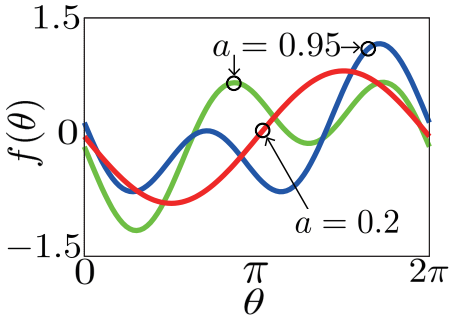

Figure 3: Theoretically obtained optimal waveforms. P is set 0.5, and a is given as $a = 0.2$ ($< 1/2$) and $a = 0.95$ ($> 1/2$) respectively. (i) For the case of $a = 0.2$, only generic solution exists (red curve). (ii) For the case of $a = 0.95$, two non-generic solutions exist (blue curve and green curve) in addition to the generic solution.

higher harmonics in the response function. Figure 2 shows variation in the shape in Z as a is increased. The balancing condition of Eq. (7) for this model is explicitly written as $\left[1 + 4a^2 \cos(\Delta\phi)\right] \sin(\Delta\phi) = 0$. For $|a| < 1/2$, there is only one (nontrivial) solution $\Delta\phi = \pi$. The optimal waveform for this generic solution is independent of a: $f_{\rm opt}(\theta) = -\sqrt{2P}\sin\theta$. Although the response function does contain second order harmonic for $0 < |a| < 1/2$, this term does not affect the shape of the optimal waveform. This finding suggests that with Z containing only weak second (or, in general even) harmonics the sinusoidal forcing is the optimal since the generic solution to balancing condition always exists. For example, for systems close to Hopf bifurcation, which contain mostly first and weak second (even) harmonics in Z, the optimal waveform is sinusoidal. However, the odd harmonics do appear, as the system goes beyond Hopf bifurcation, in the generic optimal waveform and thus systems with relatively strong third (and higher odd) harmonics are expected to retain the odd harmonics in the optimal waveform. For the generic solution the locking range is calculated as $R = \sqrt{2P}$, which is again independent of a.

In the range $|a| \geq 1/2$, we have three different solutions for the balancing condition and thus three candidates for optimal waveform. The generic solution with $\Delta\phi = \pi$ exists, however, there appear two additional, 'non-generic' solutions satisfying $\cos\Delta\phi = -1/4a^2$. For these non-generic solutions the locking ranges are identical: $R = (1 + 4a^2)\sqrt{P}/(2\sqrt{2}a) \geq \sqrt{2P}$. This shows that in the range $|a| \geq 1/2$, the non-generic optimal waveforms outperform the generic waveform; for large values of a, the improvement of locking range for the non-generic over generic waveforms increases approximately linearly. The non-generic waveforms are not purely sinusoidal and depend on the parameter a. Figure 3 shows the best optimal waveforms for the case of $a = 0.2$ ($< 1/2$) and the case of $a = 0.95$ ($> 1/2$) respectively.

We have also verified these theoretical predictions, by using a standard genetic algorithm (GA) which numerically searches for $f_{\rm opt}$. Figure 4 (a) shows all $f_{\rm opt}$ obtained by the algorithm, for both cases of full (Eq. (1)) and averaged (Eq. (2)) phase models, with $\omega = 10$, $a = 0.95$ ($> 1/2$) and $P = 0.5$ or $P = 10.0$. The numerical algorithm found the exact same optimal waveform as predicted by the theory, for both cases up to around $P = 2.0$. The numerical value of the locking range for these optimal solutions (maximum in R landscape in Figure 4 (b)) is also the same as predicted by the theory; the non-generic optimal solution performs about 23.1% better than the simple sinusoidal (generic optimal) forcing, and also it performs about 89.8% better than the pulse forcing in Figure 6. Beyond $P = 2.0$, a small discrepancy appears in the optimal waveforms obtained with the genetic algorithm. However, the shape of bimodal landscapes of $R[f]$ in Fig. 4 (b) is preserved up to around $P = 10.0$ for the case of Eq. (1), which suggests that, at least in this particular example, beyond the strictly weak forcing limit, the theoretical prediction of optimal waveform could be used as an initial candidate that can be further optimized with other techniques.

5. Applications: from van der Pol oscillators to CMOS ring oscillators

As applications of the presented theory to a more practical system, here we consider how optimal entrainment is realized for the well-known van der Pol oscillator and more practical CMOS ring oscillators, with a weak injection. The case of CMOS ring oscillators is omitted here, due to space limitation. However, this will be presented in the conference. The van der Pol oscillator is one of the most important nonlinear oscillators in electrical engineering. For instance, when we consider the injection-lock phenomena in high frequency (; RF) oscillators, the van der Pol equation provides a simplest description of the phenomena as the first approximation [28]. The system is given as the

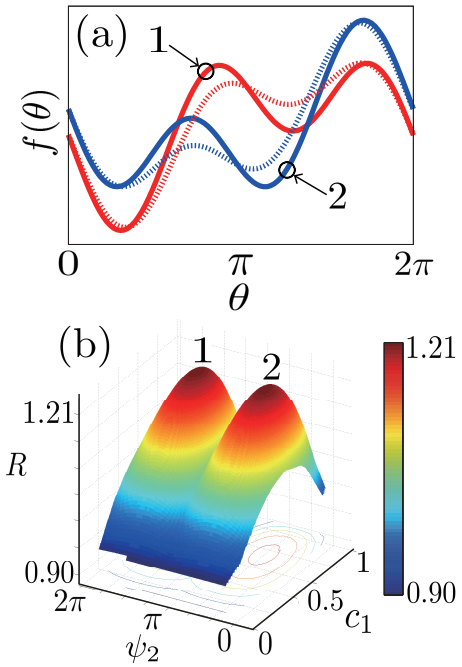

Figure 4: Optimal forcing $f_{\rm opt}$ obtained in the model with the response function of Eq. (8). Panel (a) shows all $f_{\rm opt}$, after rescaling for comparison, obtained by the genetic algorithm for $a = 0.95$: red and blue curves for $P = 0.5$ with Eq. (2), dotted curves for $P = 10.0$ with Eq. (1). In this genetic algorithm, $f_{\rm opt}$ is searched among all functions of the form $c_1 \sin\theta + c_2 \sin(2\theta + \psi_2)$. Panel (b) shows the landscape of R for $a = 0.95$ ($> 1/2$), with respect to (c_1, ψ_2). The peaks 1 and 2 of the landscape correspond to the waveforms 1 and 2 in panel (a), respectively.

following ordinary differential equation:

$$\begin{aligned} \dot{x} &= y, \\ \dot{y} &= -x + \mu(1 - x^2)y + f(\theta), \end{aligned} \tag{9}$$

where the (non-dimensionalized) variables x and y respectively represents the voltage and the current across some resistor of the oscillator. Also, we assume here the weak forcing $f(\phi)$ in the second equation of Eq. (9) is applied as an injected current. The parameter μ represent the degree of nonlinearity for the negative resistor in the oscillator. Here we choose this value as $\mu = 1.0$, for which its oscillation becomes slightly relaxational and the phase response function is obtained as in Fig. 5. Once we have obtained the phase response function $Z(\theta)$, it is now possible to design the optimal forcing of $f(\theta)$ by the presented algorithm in Sec. 3. In this particular example of moderately nonlinear oscillation, $Z(\theta)$ can be approximated as

$$Z(\theta) \sim \sum_{n=0}^{3} (a_n \cos n\theta + b_n \sin n\theta). \tag{10}$$

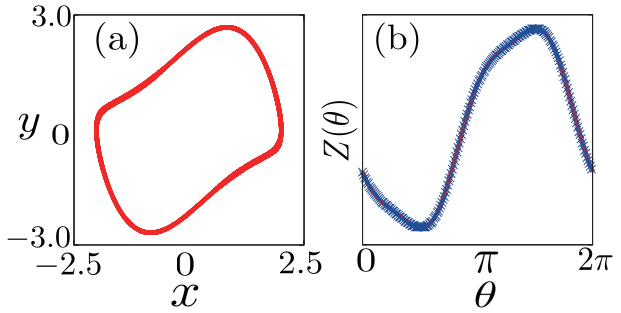

Figure 5: Limit-cycle oscillation and phase response function in the modelately nonlinear van der Pol oscillator ($\mu = 1.0$). Panel (a) shows the limit-cycle oscillation in the (x, y)-plane. Panel (b) shows the phase response function obtained from small phase shifts (×) by applying a small impulse [29]. (The applied impulse is shown in Fig. 6.) The approximated phase response function (red curve) is obtained by the least squares fitting to the Fourier series up to the third harmonics.

Then, the balancing condition $\langle Z'(\theta + \Delta\phi)Z(\theta)\rangle = 0$, which determines the unknown $\Delta\phi$ in the optimal forcing $f_{\rm opt} = \sqrt{P/Q}\{Z(\theta + \Delta\phi) - Z(\theta)\}$, is explicitly obtained with a straightforward calculation as

$$\sin(\Delta\phi)\{\cos^2(\Delta\phi) + \alpha\cos(\Delta\phi) + \beta\} = 0, \tag{11}$$

where α and β are given as $\alpha = (a_2^2 + b_2^2)/3(a_3^2 + b_3^2)$ and $\beta = (a_1^2 + b_1^2)/12(a_3^2 + b_3^2) - 1/4$ respectively. Since the coefficients in Eq. (10) are respectively obtained as $a_0 = 7.68 \times 10^{-3}$, $(a_1,\ b_1) = (-1.68 \times 10^{-1},\ -5.07 \times 10^{-1})$, $(a_2,\ b_2) = (9.29 \times 10^{-5},\ 1.61 \times 10^{-3})$, and $(a_3,\ b_3) = (-6.10 \times 10^{-2},\ 1.57 \times 10^{-2})$, α and β are respectively obtained as $\alpha = 3.02 \times 10^{-3}$ and $\beta = 8.29 \times 10$. Then, Eq. (11) is reduced to $\sin(\Delta\phi) = 0$ since $\alpha^2 - 4\beta < 0$. From $\sin(\Delta\phi) = 0$, $\Delta\phi$ is obtained as 0 or π. Since $\Delta\phi = 0$ corresponds to the trivial solution as mentioned in Sec. 3, the solution of Eq. (11) is uniquely determined as $\Delta\phi$ is π. Thus, for this example, the only possible optimal forcing is obtained as

$$f_{\rm opt}(\theta) = \sqrt{\frac{P}{Q}}\{Z(\theta + \pi) - Z(\theta)\} \tag{12}$$

This theoretical prediction is also tested by the genetic algorithm (GA) mentioned in Sec. 4, as follows. For this example, $f_{\rm opt}$ is searched among all functions of the form $c_1 \sin\theta + c_2 \sin(2\theta + \psi_2) + c_3 \sin(3\theta + \psi_3)$. We find that GA quickly converges to any functions with $c_2 = 0$, $c_1 \neq 0$, and $c_3 \neq 0$. The reason for this convergence to $c_2 = 0$ is now clear. Since this unique optimal forcing Eq. (12) has $\mathbb{Z}_2$ symmetry and all even harmonics vanish, then $c_2 = 0$ and GA search approaches such functions quickly. Figure 7 shows the landscape of R with respect to (c_1, ψ_3). As we see in Fig. 7, the landscape has only one peak and we have

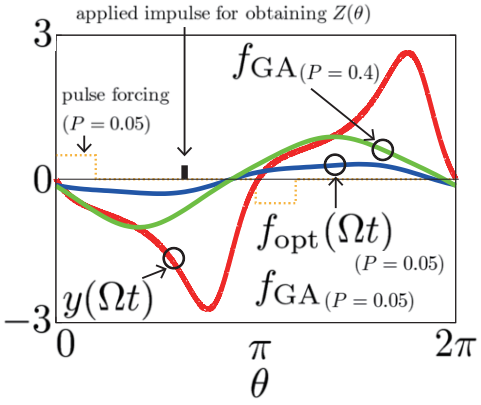

Figure 6: Optimal forcing waveform f_{opt} and other forcing waveforms. f_{opt}: theoretically obtained optimal forcing waveform ($P = 0.05$). f_{GA}: optimal forcing waveform obtained by GA ($P = 0.05$, $P = 0.4$). Note that f_{GA} perfectly matches to f_{opt} at $P = 0.05$. Here we also plot the applied impulse (width=0.05 [rad], height=+0.25) for obtaining $Z(\theta)$, the pulse forcing (width=$2\pi/10$ [rad], amplitude=0.5), and the oscillation waveform of $y(\Omega t)$ in the (entrained) van der Pol oscillator.

verified this peak always corresponds to f_{opt} in Eq. (12), when P is less than a certain value (~ 0.171). Beyond this value, the landscape of R still has the same structure with only one peak. However, this peak corresponds to a slightly deformed waveform from f_{opt} in Eq. (12), shown as f_{GA} in Fig. 6.

Summarizing these observations, the theoretically obtained optimal forcing f_{opt} to the van der Pol oscillator is valid under low power injections (; $P < 0.2$).

6. Conclusion

Construction of optimal injection waveform for entrainment was proposed and tested here with a single oscillator. The method, however, can be extended to a group of interacting oscillators where effects related to the collective phase response function [27] shall be considered. The optimal signal can also be applied in closed-loop feedback systems along with synchronization engineering [26] for seeking optimal target dynamics. A limitation of the methodology is the requirement for weak forcing so that phase models can be applied. This limitation leads to an extension of the method where the injection signal is limited to small values. These extensions, along with other targets that consider stability and basin of attraction with/without environmental noises, will be considered in a forthcoming publication. The proposed methodology provides a framework for efficient design of entrainment applications in electrical circuit technology (e.g., for injection-locked oscillators) as well as in biological pacemakers.

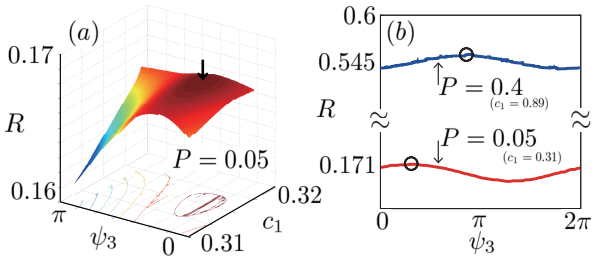

Figure 7: Landscape of R in the genetic algorithm. (a) 3D plot of the landscape. The peak is obtained at $(c_1,\ \psi_3) = (0.313,\ 0.854)$ for $P = 0.05$. The corresponding f_{GA} with $(c_1\ \psi_3) = (0.313,\ 0.854)$ is plotted in Fig. 6. (b) 2D section of the landscape. The peak is obtained at $(c_1,\ \psi_3) = (0.313,\ 0.854)$ and $(c_1,\ \psi_3) = (0.893,\ 2.986)$, respectively for $P = 0.05$ and $P = 0.4$. The corresponding f_{GA} with $(c_1,\ \psi_3) = (0.893,\ 2.986)$ is plotted in Fig. 6.

References

[1] A. S. Pikovsky, M. G. Rosenblum, and J. Kurths, *Synchronization- A Universal Concept in Nonlinear Sciences* (Cambridge University Press, Cambridge, U. K., 2001).

[2] A. T. Winfree, *The Geometry of Biological Time* (Springer-Verlag, New York, 1980).

[3] L. Glass, Chaos **1**, 13, 1991; R. A. Gray, Chaos **12**, 941, 2002.

[4] K. Yamamoto and M. Fujishima, in Proc. IEEE International Solid-State Circuits Conference, pp. 600-601, 2006.

[5] K. Takano, M. Motoyoshi, and M. Fujishima, IEEE Trans. Electronics, vol. E91-C, No. 11, pp. 1738-1743, 2008.

[6] R. Adler, in Proc. IEEE, vol. 61, pp. 1380-1385, 1973.

[7] A. Hajimiri and T. H. Lee, IEEE J. Solid-State Circuits, vol. 33, pp.179-194, 1998.

[8] G. B. Ermentrout, R. F. Galan, and N. N. Urban, Phys. Rev. Lett. **99**, 248103, 2007.

[9] A. E. Granada and H. Herzel, PLoS One **4**, e7057, 2009.

[10] N. Bagheri, J. Stelling, and F. J. Doyle, PLoS Comput. Biol. **4**, e10001014, 2008.

[11] D. Forger and D. Paydarfar, J. Theoret. Biol. **230**, 521, 2004.

[12] D. Lebiedz *et al.*, Phys. Rev. Lett. **95**, 108303, 2005.

[13] V. Gintautas and A. W. Hübler, Chaos **18**, 033118, 2008.

[14] J. Moehlis, E. Shea-Brown, and H. Rabitz, J. Comput. Nonlin. Dyn. **1**, 358, 2006.

[15] J. Ritt, Phys. Rev. E. **68**, 041915, 2003.

[16] J. Feng and H. C. Tuckwell, **91**, 018101, 2003.

[17] R. E. Best, *Phase-Locked Loops: Design, Simulation, and Applications* (McGraw-Hill, New York, 1997).

[18] A. T. Winfree, J. Theor. Biol. **16**, 15, 1967.

[19] Y. Kuramoto, *Chemical Oscillators Waves and Turbulence* (Dover, Mineola New York, 2003).

[20] In this Letter we focus on the $1:1$ resonant case. However, the presented theory is extended for general $m:n$ resonant cases.

[21] S. H. Strogatz, *Nonlinear Dynamics and Chaos* (Addison Wesley, Reading, MA, 1994), p. 105.

[22] There may be multiple locking ranges for f. For graphical examples, see [19], p. 64. In our setting, the largest range should be chosen for maximizing R in these situations.

[23] Here f are continuous and have continuous first derivatives, which belong to a function space with the norm $\|\cdot\|$ defined by $\|f\| = \max|f(\theta)| + \max|f'(\theta)|$. For details, see Chap. 1 in [24].

[24] I. M. Gelfand and S. V. Fomin, *Calculus of Variations* (Dover, Mineola New York, 2000).

[25] The existence of the generic solution to balancing condition can be proven by partially integrating $Z'(\theta+\pi)Z(\theta)$ resulting in $\langle Z'(\theta+\pi)Z(\theta)\rangle = 0$. Note that this solution has $\mathbb{Z}_2$ symmetry.

[26] I. Z. Kiss *et al.*, Science **316**, 1140858, 2007.

[27] Y. Kawamura *et al.*, Phys. Rev. Lett. **101**, 024101, 2008.

[28] R. A. York *et al.*, IEEE Trans. MTT **41**, 10, 1993.

[29] R. F. Galan, G. B. Ermentrout, and N. N. Urban, Phys. Rev. Lett. **94**, 158101, 2005.